Pulsating wave propagation in reactive flows: Flow-distributed oscillations

Mads Kærn and Michael Menzinger
Department of Chemistry, University of Toronto, 80 St. George Street, Toronto, Ontario, Canada M5S 3H6
(Received 22 July 1999; revised manuscript received 16 September 1999)

Stationary waves in a reactive flow with equal transport coefficients were recently generated by passing the oscillating Belousov-Zhabotinsky reaction medium through a tubular packed bed reactor while keeping the concentrations constant at the inflow boundary [M. Kærn and M. Menzinger, Phys. Rev. E **60**, 3471 (1999)]. Here we study the effects of oscillatory boundary conditions, and observe traveling wave fronts that propagate in either a pulsating or a steady manner. The present experiment is isothermal and conditions are such that all species have identical transport properties. This excludes rapid thermal or activator diffusion and the wave pulsation appears to be induced by an essentially kinematic mechanism. Our experimental findings are supported by numerical simulations of the full reaction-diffusion-advection system using a realistic kinetic model. Finally, the kinematic essence of the mechanism inducing wave pulsation is captured in an iterative one-variable map.

PACS number(s): 05.45.−a, 47.70.−n, 82.20.−w

I. INTRODUCTION

It was recently predicted [2] that stationary and traveling waves can form when a chemical reaction, in which all species have equal diffusion coefficients, is subject to a uniform flow. A simple kinematic model [1] explains these structures as flow-distributed oscillations which take the form of stationary waves when the phase is fixed, and of traveling waves when the phase oscillates at the inflow boundary. We have experimentally verified the formation of stationary waves [1]. The previous and present experiments involve a tubular packed bed reactor that is fed by the outflow of a continuously stirred tank reactor (CSTR). We refer to the tubular reactor as the flow domain (FD) and to the CSTR, which sets the boundary condition of the FD, as the flow domain boundary (FDB). When a volume element leaves the FDB and moves into the FD, the kinetic conditions essentially change to those of a batch reactor. In our earlier experiment [1], the FDB was in a stationary state while the FD oscillated autonomously. This was achieved by maintaining the inverse residence time k_0 in the CSTR above a critical value k_0^c below which the CSTR oscillated, as described by a bifurcation diagram in Ref. [1].

Here we study the traveling waves that arise when the boundary condition at the FDB oscillates at subcritical $k_0 < k_0^c$. At k_0 well below k_0^c we observe waves that travel upstream with an almost constant rate. If, however, k_0 lies close to the critical value, the wavefronts propagate with an oscillatory velocity. To the best of our knowledge, this is the first observation of pulsating waves in an isothermal reaction-advection system. Oscillatory waves are well established in combustion [3] and in self-propagating, exothermic polymerization fronts [4]. In these systems, the oscillatory wave velocity arises from preheating of reagents ahead of the wavefront due to the high diffusivity of heat generated within the reaction zone. Due to the interplay of diffusion and reaction they are dynamic in origin. Oscillatory wave propagation has also been predicted theoretically in an isothermal autocatalytic chemical reaction [5,6] where the pulsating mode arises due to differential diffusivities and high reaction orders. Its mechanism is essentially the same as in combustion.

In the present isothermal experiment all species have the same transport properties due to turbulent flow in the packed bed [7]. Symmetry breaking induced by differential transport [8,9] and combustionlike mechanisms [4,6] can therefore be excluded. Our experimental results are confirmed numerically using a three-variable kinetic model of the ferroin-catalyzed Belousov-Zhabotinsky (BZ) reaction [10], both in the presence and absence of diffusion. We observe that the wave pulsation is more pronounced in the absence of diffusion, indicating that its origin is kinematic. Finally, we capture the kinematic essence of the mechanism in a one-variable iterative map model.

II. EXPERIMENT

A 10×800 mm^2 glass tubular flow reactor was filled with 1 mm glass beads to create a plug flow profile. The free volume of the packed bed was 0.21 ml/cm. The flow reactor was fed by the outflow of a 4.5 ml CSTR. Its inverse residence time k_0, set by a peristaltic pump, served as the control parameter. The concentrations in the premixed feed-stream were $[\text{ferroin}]=7.5\times10^{-4}M$, $[\text{malonic acid}]=0.4M$, $[\text{bromate}]=0.2M$, and $[\text{sulfuric acid}]=0.15M$. The CSTR was monitored by a Pt electrode connected to a double junction Ag/AgCl electrode, placed in the premixed feed-stream prior to the CSTR.

The flow tube was mounted vertically on a back-lit milk-glass plate and monitored by a charge coupled device camera equipped with a 450–550 nm bandpass filter. The camera output was digitized at a rate of four frames per minute.

III. RESULTS

At $k_0 \lesssim 5\times10^{-3}$ s^{-1} the CSTR executed high amplitude relaxation oscillations. Figures 1 and 2 show the traveling waves observed at $k_0=4.0\times10^{-3}$ s^{-1} and $k_0=2.9\times10^{-3}$ s^{-1}, respectively. Each vertical frame is an actual snapshot of the flow reactor taken at 15 s intervals, with the first

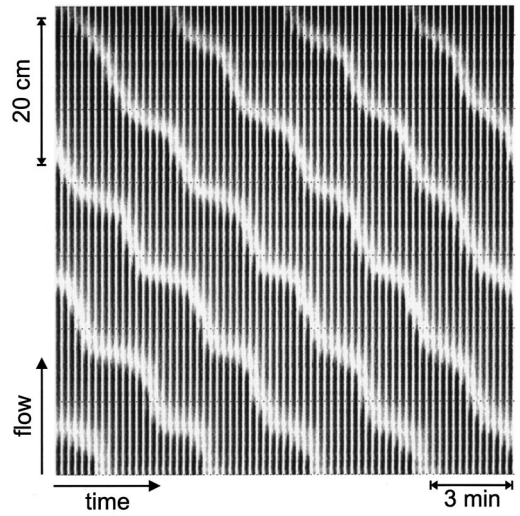

FIG. 1. Oscillatory wavefront propagation at $k_0 = 4.0 \times 10^{-3}\ \mathrm{s}^1$. Dark bands correspond to high ferroin concentrations. The flow tube (FD) is fed by an oscillatory CSTR (FDB) located below the FD. k_0 is lower than but close to the critical flow rate k_0^c where the FDB becomes stationary through a Hopf bifurcation.

snapshot at the left. The FD is fed from the bottom. Dark bands correspond to high ferroin concentrations.

The traveling waves (Figs. 1 and 2) are initiated at the outflow port of the FD (top) and they propagate upstream with an increasing intensity. The waves in Fig. 1 propagate in a pulsating manner and each wave train consists of two types of segment: a phase of slow propagation alternates with a phase of rapid propagation, giving a staircase-shaped curve in space-time. The staircases belonging to different wavefronts are nested so that all slow and fast phases align perfectly along lines of constant space and time. This gives rise to a double periodicity; a horizontal periodicity along the time axis and a spatial, vertical periodicity along the length of the FD. Finally, the amplitude of the velocity oscillation is observed to increase close to the FDB. Similar experiments which used 3 mm instead of 1 mm beads [1], under otherwise identical experimental conditions, also showed pulsating wave propagation but with decreased amplitude (not shown).

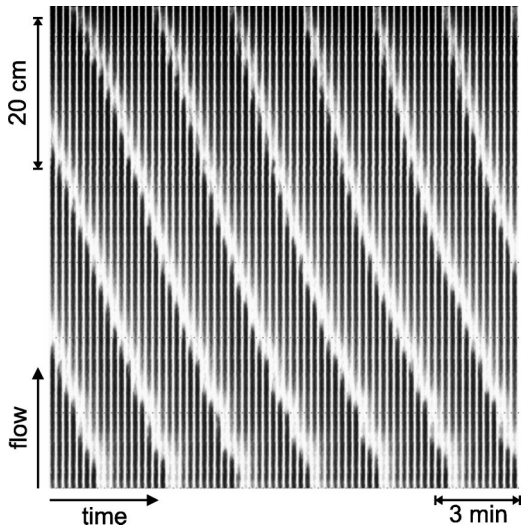

FIG. 2. Smooth wavefront propagation at $k_0 = 2.9 \times 10^{-3}\ \mathrm{s}^{-1}$ (see Fig. 1).

In contrast to the oscillatory waves in Fig. 1, those in Fig. 2, obtained at the lower value of $k_0 = 2.9 \times 10^{-3}\ \mathrm{s}^{-1}$, travel with a rather constant rate. The velocity is somewhat greater at the outflow of the FD (top) and a slight pulsation is discernible near the FDB. In summary, increasing k_0 increases the amplitude of the velocity oscillation (Fig. 1) and decreases the average rate of (backward) propagation.

IV. SIMULATIONS

We use the following three-variable model of the ferroin-catalyzed BZ reaction [10]:

$$\begin{aligned} \frac{dX}{dt} &= k_1 HAX - 2k_4 HX^2 - k_5 HXY + k_7 HAY \equiv F(X,Y,Z), \\ \frac{dY}{dt} &= \frac{q k_8 BZ}{H(C-Z)} - k_7 HAY - k_5 HXY + k_9 B \equiv G(X,Y,Z), \\ \frac{dZ}{dt} &= 2k_1 HAX - \frac{k_8 BZ}{H(C-Z)} \equiv H(X,Y,Z), \end{aligned} \tag{1}$$

where the variable concentrations are $X = [\mathrm{HBrO_2}]$, $Y = [\mathrm{Br}^-]$, $Z = [\mathrm{Fe(phen)}_3^{3+}]$ and constant concentration are $A = [\text{bromate}]$, $B = [\text{malonic acid}]$, $C = [\text{ferroin} + \text{ferriin}]$, $H = [\mathrm{H}^+]$. To model the BZ reaction in the well-stirred CSTR, the chemical kinetics is augmented by flow terms:

$$\frac{d\mathbf{X}}{dt} = \mathbf{F}(\mathbf{X}) - k_0(\mathbf{X} - \mathbf{X}_0), \tag{2}$$

where k_0 is the inverse residence time and $\mathbf{X}_0 = \{X_0, Y_0, Z_0\}$ are the feed-stream concentrations. The CSTR forms the upstream boundary ($x = 0$) of the FD. In the FD, the model must be augmented with transport terms and the dynamics is then given by

$$\frac{d\mathbf{X}}{dt} = \mathbf{F}(\mathbf{X}) + D\frac{\partial^2 \mathbf{X}}{\partial x^2} - v\frac{\partial \mathbf{X}}{\partial x}, \tag{3}$$

where D and v are the diffusion coefficient and the linear flow rate, respectively. Note that all species have identical transport coefficients. In the general case $D > 0$ we use Eq. (3) in a finite-difference scheme with zero-flux boundary conditions and CSTR concentrations [determined from Eq. (2)] at the upstream FDB. In the special case of $D = 0$ the FD is regarded as a string of independent subvolumes, each behaving like a batch reactor [Eq. (1)] that moves downstream at velocity v. In this case the concentrations of a subvolume that enters the FD are obtained from Eq. (2). The rate constants used [10] were $k_1 = 100 M^{-1}$, $k_4 = 1.7 \times 10^4 M^{-1}\ \mathrm{s}^{-2}$, $k_5 = 10^7 M^{-2}\ \mathrm{s}^{-1}$, $k_7 = 15.0 M^{-2}\ \mathrm{s}^{-1}$, $k_8 = 2.0 \times 10^{-5} M\ \mathrm{s}^{-1}$, $k_9 = 10^{-6}\ \mathrm{s}^{-1}$, and $q = 0.5$.

At the beginning of a simulation the concentrations were the same at the FDB and throughout the FD. These uniform initial conditions give rise to a spatially uniform oscillation in the FD (vertical lines in Fig. 3). In the special but artificial case where the CSTR behaves like a batch reactor ($k_0 = 0$) it

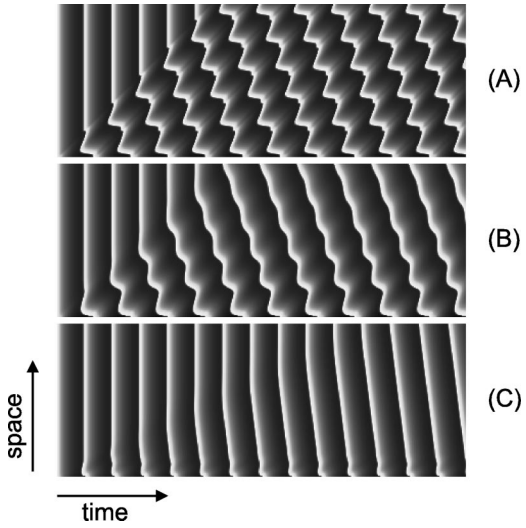

FIG. 3. Numerical simulations in one spatial dimension (vertical). Parameters used $A=0.2M$, $B=0.4M$, $H=0.15M$, $C=7.5\times10^{-4}M$, $X_0=Z_0=0M$, $Y_0=6.0\times10^{-5}M$. The inverse residence time in the CSTR was $k_0=0.05\ s^{-1}$ in (a), (b) and $k_0=0.025\ s^{-1}$ in (c). The three systems have widths of 150 (dimensional) space units Δx (arbitrary length) and were integrated for a total of 400 s (horizontal). In (a) and (b) the linear flow rates were $v=\Delta x$/s to achieve identical resolutions in space and time whereas the linear flow rate in (c) was halved. Panel (a) is obtained in the absence of diffusion while $D=\Delta x^2$/s in (b) and (c).

can be shown that the uniform oscillation persists even in the presence of a flow. However, when $k_0>0$ the phase-plane portrait and the period (T') of the CSTR oscillation are different from that of the batch reactor (T) and the out-of-phase oscillation at the FDB breaks the spatial uniformity within the FD (see Fig. 4 and discussion below). Figure 3(a) shows traveling waves emerging when $k_0=0.05\ s^{-1}$ and diffusion is neglected. While the envelope of the wave travels upstream, the wavefront propagation is significantly different from that observed experimentally (Figs. 1 and 2). Instead of being initiated at the outflow port (top) the waves are periodically emitted from, ''organizing centers'' located at fixed spatial locations separated by the distance $\lambda=vT$. Pairs of waves, one traveling rapidly downstream and the other traveling slowly upstream, are emitted from these centers with a period coinciding with that at the FDB.

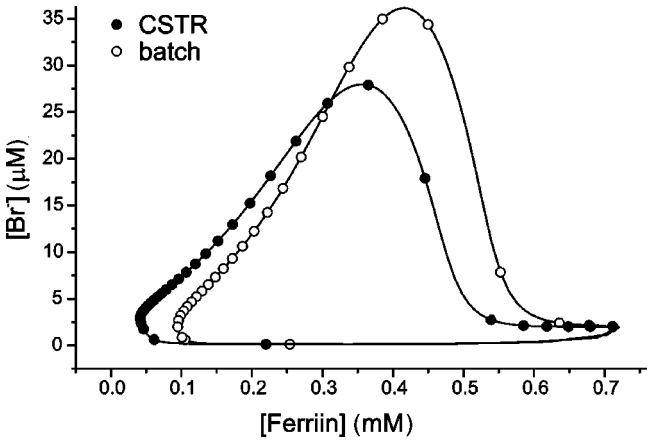

FIG. 4. Phase portraits of the $T\sim28$ s batch mode and $T'\sim37$ s CSTR limit cycles. Circles indicate progression at equal time intervals.

Figure 3(b) shows the traveling wave that is formed at the same residence time as in Fig. 3(a) but in the presence of diffusion. In the upper part of the FD, waves are initiated at the outflow port (top) and they propagate upstream with an oscillatory velocity whose amplitude increases as the wavefront approaches the FDB, as observed experimentally (Fig. 1). However, close to the FDB waves are emitted periodically from organizing centers as observed in Fig. 3(a). As one would expect, diffusion homogenizes the local oscillators and makes the wavefronts propagate more smoothly farther from the FDB. Finally, in the simulation presented in Fig. 3(c), k_0 is halved. As a result, the wave propagates upstream with a constant velocity far from the FDB while close to the FDB the wave velocity oscillates slightly, in good agreement with the experiments (Fig. 2). Note that the average wave velocity in Fig. 3(c) is greater than that at the higher throughput in Fig. 3(b), in agreement with the experimental observations in Figs. 1 and 2.

V. MECHANISM OF WAVE PULSATION

As mentioned above, the cause of traveling FDO waves is the difference in oscillation periods at the FDB and in the FD. Since these waves are essentially kinematic and diffusion appears not to play a key role, only the case $D=0$ will be discussed further. The local velocity ν of a phase wave is given by

$$\nu=-\left(\frac{\partial\phi}{\partial t}\right)_x\left(\frac{\partial x}{\partial\phi}\right)_t,$$

where $(\partial\phi/\partial t)_x$ is the rate of change of the phase at location x and $(\partial\phi/\partial x)_t$ is the phase gradient at time t. The observed wave pulsation arises from a nonuniform variation of these two factors in space and time. We will show that the forcing of the FD by the FDB oscillator accounts for the nonuniform, segmented time and space dependence of the phase wave velocity along the FD.

When a volume element leaves the FDB and enters the FD it crosses the boundary between the two distinct kinetic domains: one with $k_0>0$ (the CSTR) and the other with $k_0=0$ (batch reactor in the flow tube). Figure 4 shows the calculated phase portraits of cycles at the FDB and in a volume element moving through the FD. The progression through one cycle is indicated by marks every 2 s. While both cycles slow down at low ferriin and bromide concentrations, the slowing down of the FDB (CSTR) oscillation is particularly pronounced. We note that while the two limit cycles coincide for $k_0=0$, the differences of phase plane portraits and oscillation periods between FDB and FD become more pronounced for higher values of k_0.

To capture the kinematic essence of the different limit cycles at the FDB and in the FD we introduce a one-variable iterative map of sawtooth oscillations in one spatial dimension. The spatial dimension is divided into grid points $i=0,1,\ldots$ with the FDB located at $i=0$ and the FD spanning all $i>0$. The value of the phase variable $y_i(t)$ at location $i>0$ and time step t is given by

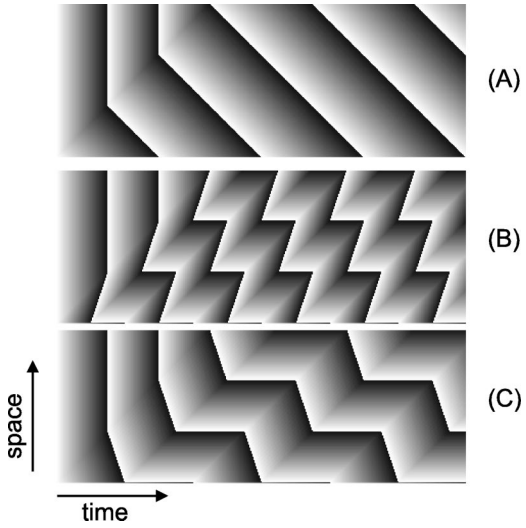

FIG. 5. Spatiotemporal behavior generated when a sawtooth oscillation is carried through the FD at a constant rate and is periodically forced at the boundary. The kinetic constants a,b are fixed in the FD, while kinetic constants a',b' at the FDB are different in (a), (b), (c) (see text). (a) identical attractors ($b=b'$) and different periods ($T'=2T$) give waves traveling steadily upstream. Different attractors ($b\neq b'$) and periods ($T'\neq T$) give a segmented wave velocity: (b) downstream and stationary wavefronts are emitted from organizing centers [cf. Fig. 3(a)], (c) upstream traveling and stationary waves are emitted [cf. Figs. 1 and 3(b)].

$$y_i(t)=\begin{cases} y_{i-1}(t-1)+a \quad \text{if} \quad 0\leqslant(y_{i-1}(t-1)+a)<b \\ 0 \quad \text{otherwise,} \end{cases} \tag{4}$$

where a and b are kinetic constants. The value of y at $i=0$ is also given by Eq. 4 but with a different set of kinetic constants a' and b' and without the spatial component. This corresponds exactly to the situation in Fig. 3(a) where the two oscillations had different values of the kinetic constant k_0: Eq. (2) with $k_0>0$ at the FDB and $k_0=0$ in the FD. With the above construction, the autonomous oscillator at $i=0$ has period $T'=b'/a'$ while a different oscillator with period $T=b/a$ is transported through the FD at a velocity of one grid point per time step. The attractors at the FDB and in the FD are the lines extending from $y=0$ to $y=b'$ and $y=b$, respectively. Although the above map appears to be relatively simple, its coupling to the forcing oscillator at $i=0$ may cause the spatiotemporal behavior within the FD to become rather complex.

Figure 5 shows the space-time plots for fixed kinetic constants in the FD ($a=0.01$, $b=0.5$, $T=50$) and for three sets of kinetic constant a',b' at the FDB. As in Fig. 3 the FD is initially homogeneous and a spatially uniform oscillation with period $T=50$ is observed. The spatial symmetry may be broken as the map is iterated, provided that the FDB and the FD oscillators have different periods and/or attractors. In Fig. 5(a) the FDB oscillator has kinetic constants $a'=0.005$, $b'=0.5$ and the two attractors coincide ($b'=b$), but oscillate with different periods ($T'=100$, $T=50$). As shown in Table I the local change in phase is $(\partial\phi/\partial t)_x=a'$ while the phase gradient is eventually constant throughout the FD and is given by $(\partial\phi/\partial x)_t=a-a'$. Hence the phase wave travels upstream with the constant velocity $\nu=-a'/(a-a')=-1$.

TABLE I. Phase values [$y_i(t)$ values] at the FDB ($i=0$) and in the FD ($i>0$) during five iterations of Eq. (4) when $y_0(0)=0$ and $y_0(t)<b'$, $y_i(t)<b$. The phase gradient equals $a-a'$.

$i=5$						$5a$
$i=4$					$4a$	$4a+a'$
$i=3$				$3a$	$3a+a'$	$3a+2a'$
$i=2$			$2a$	$2a+a'$	$2a+2a'$	$2a+3a'$
$i=1$		a	$a+a'$	$a+2a'$	$a+3a'$	$a+4a'$
$i=0$	0	a'	$2a'$	$3a'$	$4a'$	$5a'$
	$t=0$	$t=1$	$t=2$	$t=3$	$t=4$	$t=5$

When the attractors in the two domains do not coincide ($b\neq b'$), a nonuniform phase gradient is formed along the FD as follows. In the case where $b'>b$, any value of y_o at the FDB greater than b at time $t-1$ causes y_1 to be set to zero at $i=1$ in the following time step, i.e., $y_1(t)=0$ if $y_0(t-1)>b$. Hence, $y_1=0$ during $n=T'(b'-b)$ successive time steps. This is illustrated in Table II which is a continuation of Table I for $t>5$. It is assumed that $b=6a'$ such that $y_1(t>6)=0$, $y_2(t>7)=a$, etc. The resetting of $y_1(t)$ introduces a new temporal and spatial periodicity in the FD: n subsequent grid points have y values separated by increments of a and $y_{i>0}(t)$ remains constant during n successive time steps. The remaining $m=T'-n$ grid points have y values separated by increments of $a-a'$. The phase gradient is therefore segmented into alternating regions of length n and m where the phase gradient is a and $a-a'$, respectively. As a result, the velocity of the phase wave changes in a discontinuous fashion: During m time steps the wavefront propagates with a finite velocity $\nu=-a'/(a-a')$, since $(\partial\phi/\partial t)_x=a'$ and $(\partial\phi/\partial x)_t=a-a'$. During the following n time steps the velocity is $\nu=0$ since the phase remains constant and $(\partial\phi/\partial t)_x=0$.

Figures 5(b) and 5(c) show the space-time plots for $a'=0.015$, $b'=1.0$, and $a'=0.0075$, $b'=1.0$, respectively. Figure 5(b) reproduces the qualitative behavior seen in Fig. 3(a), in particular, pairs of traveling waves are emitted periodically from organizing centers, one moving downstream ($a'>a$, $\nu=3$) and the other stationary. The temporal oscil-

TABLE II. Continuation of Table I for $5<t<12$. It is assumed that $b=6a'$ such that $y_1(t>6)=0$. The point $y_1(t=7)=0$ corresponds to the cusp-shaped organizing center in Fig. 5(c), emitting an upstream traveling and a stationary wave. At $t=6$ the phase gradient equals $a-a'$ while at $t=11$ it equals a. For $b'>b$ the FD is segmented into alternating regions of length $n=(b'-b)/a'$ and $m=T'-n$ where the phase gradient is a and $a-a'$, respectively.

$i=5$	$5a+a'$	$5a+2a'$	$5a+3a'$	$5a+4a'$	$5a+5a'$	4a
$i=4$	$4a+2a'$	$4a+3a'$	$4a+4a'$	$4a+5a'$	$3a$	$3a$
$i=3$	$3a+3a'$	$3a+4a'$	$3a+5a'$	$2a$	$2a$	$2a$
$i=2$	$2a+4a'$	$2a+5a'$	a	a	a	a
$i=1$	$a+5a'$	0	0	0	0	0
$i=0$	$6a'$	$7a'$	$8a'$	$9a'$	$10a'$	$11a'$
	$t=6$	$t=7$	$t=8$	$t=9$	$t=10$	$t=11$

lation at a fixed point in the FD is segmented into two phases, one with constant phase the other with $(\partial\phi/\partial x)_t = a - a'$, each occupying half of the FDB period T' in agreement with $b' = 2b$. While the temporal periodicity of the organizing centers is T', the spatial distance between organizing centers coincides with the periodicity of the FD oscillation which was also observed in Fig. 3(a). Finally, Fig. 5(c) reproduces the qualitative features of the pulsating wave propagation observed experimentally. In this case the wavefront is initiated at the exit boundary of the flow domain and propagates with an segmented velocity as in Fig. 5(b). However, since $a' < a$ the direction of the traveling phase wave is upstream ($\nu = -3$) in qualitative agreement with Fig. 1.

VI. DISCUSSION

We report here an experimental observation of wavefronts propagating with an oscillatory velocity in an isothermal chemical reaction-diffusion-advection system. The conditions are such that the oscillatory velocity cannot be explained by rapid thermal or activator diffusion [3–6]. The pulsating wavefronts are the result of a purely kinematic mechanism based on differences between the limit cycle attractors in the flow tube (the FD) and at the inflow boundary (the FDB). In the present experiment, this difference is primarily a pronounced slowing down of a certain phase of the FDB oscillation. Volume elements entering the flow tube during the slow phase of the FDB have almost identical phase values. This causes the phase gradient across the flow tube to become nonuniform and segmented into alternating regions corresponding, roughly, to volume elements that entered during the slow phase and those that did not. This segmented phase gradient causes the phase wave to propagate with an oscillating velocity.

We have captured the essential kinematics of pulsating and smoothly traveling FDO waves using a one-variable iterative map model in one spatial dimension. In this model, smoothly traveling waves emerge [Fig. 5(a)] when the attractors coincide ($b = b'$) but have different periods ($T' \neq T$), while pulsating waves are formed when $T' \neq T$ and $b' \neq b$ [Figs. 5(b) and 5(c)]. While the latter corresponds to our experimental condition (Fig. 4) an oscillatory wave velocity is expected more generally whenever a nonlinear phase gradient is established. This may occur even when the attractors coincide if one is subject to local slowing down as opposed to the global slowing down used in Fig. 5(a). A constant wave velocity is therefore expected to occur only if the phase value of the forcing oscillator at the FDB is linearly mapped into a phase gradient in the FD, while oscillating wave propagation is expected if this mapping is nonlinear. The amplitude of the oscillation increases as the mapping becomes more nonlinear. Indeed the experimentally observed pulsation is more pronounced at higher values of k_0 (Figs. 1 and 2). On the other hand, diffusion tends to diminish the phase gradient and experiments with larger glass beads [1] and an increased turbulent diffusion coefficient show a decreased amplitude of velocity oscillations.

ACKNOWLEDGMENTS

This work was funded by Grant No. RGPIN5783-98 of the NSERC of Canada. M.K. received financial support from the Danish Research Academy.

[1] M. Kærn and M. Menzinger, Phys. Rev. E **60**, 3471 (1999).
[2] P. Andresén, M. Bache, E. Mosekilde, G. Dewel, and P. Borckmans, Phys. Rev. E **60**, 297 (1999).
[3] K. G. Shkadinskii, B. I. Khalin, and A. G. Merzhanov, Combust., Explos. Shock Waves **1**, 15 (1973).
[4] S. E. Solovyov, V. M. Ilyashenko, and J. A. Pojman, Chaos **7**, 331 (1997).
[5] M. J. Metcalf, J. H. Merkin, and S. K. Scott, Proc. R. Soc. London, Ser. A **447**, 155 (1994).
[6] N. J. Balmforth, R. V. Craster, and S. J. A. Malham, Proc. R. Soc. London, Ser. A **455**, 1401 (1999).
[7] G. F. Froment and K. B. Bischoff, *Chemical Reactor Analysis and Design* (Wiley, New York, 1990).
[8] A. M. Turing, Philos. Trans. R. Soc. London, Ser. B **327**, 37 (1952).
[9] A.B. Rovinsky and M. Menzinger, Phys. Rev. Lett. **70**, 778 (1993).
[10] A. M. Zhabotinsky and A. B. Rovinsky, J. Phys. Chem. **94**, 8001 (1990).